Available online at www.sciencedirect.com
SCIENCE DIRECT®
Journal of Chromatography A, 989 (2003) 139–153
JOURNAL OF CHROMATOGRAPHY A
www.elsevier.com/locate/chroma

Evaluation of protein-A chromatography media

Justin T. McCue[a], Glen Kemp[b], Duncan Low[a], Igor Quiñones-García[a,*]
[a]*Millipore Corporation, BioPharmaceutical Division, 32 Wiggins Avenue, L2B, Bedford, MA 01730, USA*
[b]*Millipore Corporation, Bioprocessing Corporation Ltd., Consett, UK*

Abstract

In process-scale antibody purification, protein-A affinity chromatography is commonly used as the initial purification step. In this paper, two different protein-A media were evaluated. These adsorbents have a porous glass backbone with different pore sizes: 700 Å and 1000 Å. Adsorption equilibrium data of human immunoglobulins on these media were measured via a batch technique and correlated using the Langmuir isotherm model. A larger static capacity was found for the smaller pore size material, which is probably a result of the larger specific surface area and associated higher ligand concentration. The protein uptake kinetics were also obtained via a stirred tank experiment using different initial protein concentrations. A surface layer model was used to represent the protein uptake by the media and to estimate values of a concentration-independent effective diffusivity within the particle. Experimental breakthrough curves were also obtained from packed beds operated under different conditions. Calculated breakthrough profiles were found to be in good agreement with the experimental results. Experimental breakthrough data were used to determine the dependence of the dynamic capacity of the media as a function of the fluid residence time. A larger dynamic capacity was also found for the smaller pore size media. The permeability of large scale packed beds was also reported and used in conjunction with the dynamic capacity to calculate the process production rate.

Keywords: Adsorption isotherms; Diffusivity; Dynamic capacity; Permeability; Production rate; Preparative chromatography; Affinity adsorbents; Immunoglobulins; Protein-A; Antibodies

1. Introduction

Chromatography is a well established step in the purification of biopharmaceuticals at the process scale [1]. The use of protein-A affinity chromatography is often employed for the selective initial purification of monoclonal antibodies from clarified cell culture fluid [2–9]. Process economy and high throughput in process-scale antibody purification trains are achieved through the use of chromatography media that possess: (i) high capacity, (ii) high permeability and (iii) good chemical stability (reusable for multiple cycles). Note that operation at higher flow-rates increases productivity and minimises potential product degradation.

Several protein-A chromatography media are available, with their main difference being support matrix type. Protein-A immobilised onto matrices consisting of agarose, porous glass (PG) and ceramics are commercially available [10]. Choice of matrix composition, particle size and porosity gives rise to differences in compressibility, chemical

*Corresponding author. Fax: +1-908-820-6112.
E-mail address: igor.quinones-garcia@spcorp.com (I. Quiñones-García).

0021-9673/03/$ – see front matter
doi:10.1016/S0021-9673(03)00005-0

stability, permeability, antibody diffusivity, and binding capacity—which can all have a major effect on purification performance.

Several published studies dealt with the determination of dynamic capacity, permeability, and production rate for commercially available protein-A media [7,8]. However, there seems to be little published information [11] regarding the equilibrium and transport parameters that govern these separations, i.e. adsorption isotherms and internal diffusivities. In this paper, adsorption isotherm and uptake kinetics data were obtained in batch mode using a stirred tank set-up. Langmuir equilibrium parameters and values for the effective diffusivities were estimated from the analysis of the experimental data using suitable models. Furthermore, these parameters were used in the calculation of packed bed breakthrough profiles and dynamic capacity. Good agreement was found between calculated and experimental breakthrough results. Finally, media permeability and dynamic capacity were used to estimate the process production rate for a range of feedstock antibody titres at different residence time values.

2. Experimental

2.1. Materials

Porous glass (PG) based protein-A chromatography media were obtained from Millipore (Bedford, MA, USA). Media particle sizes were in the range of 75–125 μm. Media of two different pore sizes were examined [~700 Å (PG 700) and ~1000 Å (PG 1000)]. The properties of these materials are summarized in Table 1 [12]. Note that bulk porosity (ϵ_b) and particle porosity (ϵ_p) were estimated from the other data presented in this table, assuming a density of 2.23 g/cm^3 for the quartz skeleton. Human gammaglobulins (hIgG) were purchased from SeraCare (Oceanside, CA, USA) in the form of a 5% solution (product HS-475), and from Sigma–Aldrich (St. Louis, MO, USA) in the form of a 99% lyophilised powder (product G4386). The SeraCare material was used in the stirred tank experiments, while both materials were used in the packed bed studies. All other chemicals were analytical reagent grade and purchased from Sigma–Aldrich.

Table 1
Properties of the porous glass materials [12]

Pore size (Å)	Area (m^2/g)	Pore volume (cm^3/g)	Bulk density (g/cm^3)	ϵ_b	ϵ_p
700	35	1	0.39	0.43	0.68
1000	23	1	0.38	0.45	0.69

2.2. Procedures and equipment

2.2.1. Adsorption equilibrium data

Adsorption equilibrium data for hIgG on PG 700 and PG 1000 were determined from batch experiments. In these experiments, ~50 cm^3 of phosphate buffer saline (PBS) (pH 7.4, 10 m*M* phosphate, 0.138 *M* NaCl and 0.0027 *M* KCl) containing initial known concentrations of hIgG (0.1–3.0 mg/cm^3) were contacted with ~0.2–0.5 cm^3 of the media at room temperature. All buffers and solvents used in this study were filtered using a 0.22-μm filter (Millipore, Bedford, MA, USA). Media volume was estimated from the knowledge of the packed bed volume and the bulk porosities presented in Table 1. After equilibration, the absorbance of the solution was read at 280 nm using a EM-1 spectrophotometer from Bio-Rad (Hercules, CA, USA). Calibration curves were used to convert the spectrophotometer signal to protein concentration. The amount of protein adsorbed by the media was obtained from a material balance.

2.2.2. Protein uptake kinetics

Antibody uptake kinetics were determined from stirred tank experiments in a vessel similar to the one described elsewhere [13]. A phosphate buffered saline (PBS) solution (~50 cm^3) containing known initial concentrations of hIgG (0.1–5.0 mg/cm^3) was placed in a 200-ml flow cell apparatus (Millipore). The solution was agitated using a 5-cm long, suspended stir bar at 100 rpm. Samples of ~0.2–0.5 ml of media were injected into the agitated solution. The hIgG concentration in the solution was monitored by continuously recirculating a small stream at 10 ml/min through a EM-1 spectrophotometer from Bio-Rad, equipped with a low-volume flow cell. The

recirculating stream was drawn through a 0.65-μm membrane through the bottom of the flow cell using a peristaltic pump from Cole-Parmer (Vernon Hills, IL, USA). The total response time of the circulation loop and UV detection system was ~20 s.

2.2.3. Column chromatography

The media were packed into 0.66-cm (Omnifit, Rockville Center, NY, USA) and 1.1-cm I.D. (Millipore, Bedford, MA, USA) columns with bed heights ranging from 5.0 to 35 cm. Frontal analysis runs were performed using a BioCad 700E chromatography system (Perseptive Biosystems, Framingham, MA, USA). Antibody concentrations were monitored by UV absorbance at 280 nm. The packed columns were first equilibrated with PBS. Antibody (1.0 mg/cm^3) in PBS was then loaded onto the columns. The bound hIgG was eluted using a 0.1 *M* glycine–HCl solution (pH 3.0). The media were regenerated using H_3PO_4 (pH 1.5).

3. Theoretical

3.1. Calculation of concentration profiles for the stirred tank uptake kinetics

A surface layer representation of the protein transport within the particle proposed elsewhere [14] was adopted in this study. The advantage of this type of model is the ability to fit the experimental protein uptake data with concentration-independent effective diffusivities and to take into account the fact that film mass transfer is the limiting resistance at low concentrations. Using a single effective diffusivity value to fit uptake curves at different initial concentrations with more simple models (such as the homogeneous or pore diffusion model) has proven to be challenging [11,14]. Within the surface layer model, the transport to the surface layer is controlled by the external film mass transfer while homogeneous diffusion or pore diffusion controls at the core of the particle. The published analytical treatment [14] results in a discontinuity in the uptake rate at the time when a switch from external mass transfer control to intraparticle diffusion control occurs. Essentially, two different models are used in order to describe two different periods of the process. Our model formulation is different in the sense that a unique model holds at all times and, as a result, the discontinuity is avoided. In our case, when the thickness of the surface layer becomes negligible, the surface layer model reduces to either the homogeneous diffusion model or the pore diffusion model.

Prior work [11,13–19] has shown that the separation process in the stirred tank is typically governed by two mass transfer resistances: (i) film resistance and (ii) intraparticle resistance. For the case of protein-A media, it has been shown that pore diffusion and film mass transfer govern the overall mass transfer resistance, while contribution from the surface reaction is negligible [11]. Within the context of the surface layer model, mass transfer occurring within the particle's core can be described either by the homogeneous diffusion model or by the pore diffusion model [14]. For the particular case when the homogeneous diffusion model is used, the following conservation equation holds:

$$\frac{\partial Q}{\partial t} = \frac{D_{\text{eff}}}{(R-\delta)^2} \cdot \left(\frac{\partial^2 Q}{\partial \rho^2} + \frac{2}{\rho} \frac{\partial Q}{\partial \rho} \right) \tag{1}$$

where Q is the solute concentration within the particle core, a function of both radial position (r) and time (t). The radial position is normalised [$\rho = r/(R-\delta)$] with respect to the core radius ($R-\delta$), where δ is the thickness of the surface layer. The kinetics of intraparticle mass transfer within the core is accounted via an effective diffusion coefficient (D_{eff}). Eq. (1) reduces to the homogeneous diffusion model [14] when the thickness of the adsorption layer is negligible ($\delta = 0$), i.e.

$$\frac{\partial Q}{\partial t} = \frac{D_{\text{eff}}}{R^2} \cdot \left(\frac{\partial^2 Q}{\partial \rho^2} + \frac{2}{\rho} \frac{\partial Q}{\partial \rho} \right) \tag{2}$$

For the case when the pore diffusion model is used to describe mass transfer within the particle core, the following conservation equation holds:

$$(1-\epsilon_{\text{p}}) \cdot \frac{\partial Q_{\text{s}}}{\partial t} + \epsilon_{\text{p}} \cdot \frac{\partial C_{\text{p}}}{\partial t} = \frac{\epsilon_{\text{p}} D_{\text{p}}}{(R-\delta)^2} \cdot \left(\frac{\partial^2 C_{\text{p}}}{\partial \rho^2} + \frac{2}{\rho} \frac{\partial C_{\text{p}}}{\partial \rho} \right) \tag{3}$$

where Q_{s} is the solute concentration in the particle's solid (on a pore-free volume basis), C_{p} is the solute

concentration in the pore fluid, ϵ_p is the particle porosity, and D_p is the effective pore diffusivity. Within the context of the pore diffusion model, it is typically assumed that the adsorbed solute is at equilibrium with the pore fluid at each radial position within the particle [14]. Accordingly, Eq. (3) could be written as:

$$\left[(1-\epsilon_p)\cdot\frac{dQ_s}{dC_p}+\epsilon_p\right]\frac{\partial C_p}{\partial t}= \frac{\epsilon_p D_p}{(R-\delta)^2}\cdot\left(\frac{\partial^2 C_p}{\partial \rho^2}+\frac{2}{\rho}\frac{\partial C_p}{\partial \rho}\right) \quad (4)$$

Assuming that the Langmuir equilibrium model can be used to describe the equilibrium between the pore fluid and the solid-phase concentrations, it follows that:

$$\frac{dQ_s}{dC_p}=\frac{Q_m K_L}{(1+K_L C_p)^2} \quad (5)$$

where Q_m is the monolayer capacity and K_L is the Langmuir equilibrium constant. As in the case above, the surface layer model described by Eq. (4) reduces to the pore diffusion model [14] when the thickness of the adsorption layer is negligible ($\delta = 0$), i.e.

$$\left[(1-\epsilon_p)\cdot\frac{dQ_s}{dC_p}+\epsilon_p\right]\frac{\partial C_p}{\partial t}= \frac{\epsilon_p D_p}{R^2}\cdot\left(\frac{\partial^2 C_p}{\partial \rho^2}+\frac{2}{\rho}\frac{\partial C_p}{\partial \rho}\right) \quad (6)$$

The above equations have to be solved subject to initial and boundary conditions. The initial concentration profile in the particle's core is given by:

$$Q(\rho,0)=0 \quad (7)$$

for the homogeneous diffusion model and by

$$Q_s(\rho,0)=0 \quad (8)$$

$$C_p(\rho,0)=0 \quad (9)$$

for the pore diffusion model.

When the transport at the particle's core is described using the homogeneous diffusion model, the balance of solute flux across the film gives a boundary condition at the surface of the particle:

$$\frac{\partial Q^s}{\partial t}\cdot\left[1-\frac{(R-\delta)^3}{R^3}\right]+\frac{3D_{eff}}{R^3}(R-\delta)\left\{\frac{\partial Q}{\partial \rho}\right\}_{(1,\theta)} = \frac{3k_f}{R}\cdot(C_t-C^s) \quad (10)$$

where C_t and C^s are the liquid phase concentrations in the bulk tank fluid and at the particle's surface, respectively, and Q^s is the solute concentrations in the surface layer; k_f is the film mass transfer coefficient. The value of the film mass transfer coefficient was estimated from the following correlation [20]:

$$k_f = 2\cdot\frac{D_f}{d_p}+0.31\left(\frac{\mu}{\rho D_f}\right)^{-2/3}\cdot\left(\frac{\Delta\rho\mu g}{\rho^2}\right)^{1/3} \quad (11)$$

where D_f is the molecular diffusivity in free aqueous solution, d_p is the mean particle diameter, μ is the liquid viscosity, ρ is the liquid density, $\Delta\rho$ is the density difference between particulate and liquid and g is the gravity acceleration. We estimated a value of $k_f = 6.7\cdot 10^{-4}$ cm/s for our stirred tank experiments.

Note that the liquid phase concentration at the surface of the particle is related to the solute concentration in the surface layer via Langmuirian equilibrium:

$$C^s=\frac{Q^s}{K_L}\cdot\left[\frac{1}{Q_m-Q^s}\right] \quad (12)$$

When $\delta = 0$, Eq. (10) above reduces to the expression valid for the homogeneous diffusion model [14]:

$$\left\{\frac{\partial Q}{\partial \rho}\right\}_{(1,\theta)}=\frac{Rk_f}{D_{eff}}(C_t-C^s) \quad (13)$$

On the other hand, for the case when mass transfer in the core is described using the pore diffusion model, the following equation holds for the balance of mass flux at the particle's interface:

$$\left[1-\frac{(R-\delta)^3}{R^3}\right]\cdot\left[\epsilon_p+\frac{(1-\epsilon_p)Q_m K_L}{(1+K_L C^s)^2}\right]\cdot\frac{\partial C^s}{\partial t} + \frac{3D_p\epsilon_p}{R^3}(R-\delta)\left\{\frac{\partial C_p}{\partial \rho}\right\}_{(1,\theta)}=\frac{3k_f}{R}\cdot(C_t-C^s) \quad (14)$$

When $\delta = 0$ (no surface layer), Eq. (14) above reduces to the expression valid for the pore diffusion model [14]:

$$\left\{\frac{\partial C_p}{\partial \rho}\right\}_{(1,\theta)} = \frac{Rk_f}{D_p \epsilon_p}\cdot(C_t - C^s) \quad (15)$$

The final boundary conditions are given by the fact that there is no mass transfer at the centre of the particle. For the homogeneous diffusion model, the following expression applies:

$$\left\{\frac{\partial Q}{\partial \rho}\right\}_{(0,\theta)} = 0 \quad (16)$$

while for the pore diffusion model the following equations hold:

$$\left\{\frac{\partial Q_s}{\partial \rho}\right\}_{(0,\theta)} = 0 \quad (17)$$

$$\left\{\frac{\partial C_p}{\partial \rho}\right\}_{(0,\theta)} = 0 \quad (18)$$

Finally, the conservation equation related with the fluid phase in the tank is given by [14]:

$$\frac{dC}{dt} = -3\frac{V_m}{V_f}\frac{k_f}{R}\cdot(C_t - C^s) \quad (19)$$

where V_m and V_f are the volumes of the media and fluid in the tank, respectively. The initial condition for Eq. (19) is determined by the initial concentration of the solute (C°) in the bulk liquid:

$$C(0) = C^\circ \quad (20)$$

The solution of the equations for the different models was found via orthogonal collocation on finite elements [15]. Following discretisation, the resulting system of differential equations for each model was numerically integrated using the MATLAB routine ode15s. This routine uses a quasi-constant step size implementation of numerical differentiation formulas in terms of backward differences.

3.2. Calculation of packed bed breakthrough curves

The concentration profile in the column can also be described using mass conservation [15]. In addition to fluid film and intraparticle mass transfer resistances, the process in the column is influenced by axial dispersion. The packed bed is however assumed to be radially homogeneous, i.e. the process parameters are constant over the cross section.

The nondimensional mass balance in a column slice gives the concentration in the fluid stream as a function of both position and time, $C(z,\theta)$ as [15]:

$$\frac{\partial C}{\partial \theta} + \frac{\partial C}{\partial z} + 3\cdot\frac{1-\epsilon}{\epsilon}\frac{k_f \tau}{R}(C - C^s) = \frac{1}{Pe}\cdot\frac{\partial^2 C}{\partial z^2} \quad (21)$$

In the above equation the nondimensional position (z), nondimensional time (θ), residence time (τ), and Peclet number are defined by:

$$z = x/L \quad (22)$$

$$\theta = t/\tau \quad (23)$$

$$\tau = L/u \quad (24)$$

$$Pe = uL/D_a \quad (25)$$

In the above equations ϵ is the porosity of the packed bed, x is the actual position in the direction of the flow, L is the column length, u is the interstitial velocity, and D_a is the axial dispersion coefficient. The value of the film mass transfer coefficient was estimated from the following correlation [21]:

$$k_f = \frac{D_f}{d_p}\cdot\left[2 + 1.45\left(\frac{u_s \rho d_p}{\mu}\right)\cdot\left(\frac{\mu}{\rho D_f}\right)^{1/3}\right] \quad (26)$$

where u_s is the superficial velocity. The value of the column Pe number was estimated from a published correlation [22].

$$Pe = \frac{L}{d_p}\cdot\left[\frac{d_p u_s}{(1-\epsilon_b)D_f}\right]^{-1/6} \quad (27)$$

The initial condition corresponding to Eq. (21) is given by the profile of solute concentration along the column:

$$C(z,0) = 0 \quad (28)$$

The first boundary condition is defined by the ''close–close'' Danckwerts condition at the column inlet:

$$\left\{\frac{\partial C}{\partial z}\right\}_{(0^+,\theta)} = -Pe\left[C(0^-,\theta) - C(0^+,\theta)\right] \quad (29)$$

Note that in Eq. (29) the feed concentration at the

column inlet defines the first term within the bracket, i.e.

$$C(0^{-},\theta) = C_{\mathrm{FEED}} \tag{30}$$

The second boundary condition is defined by the stop of mass transfer at the column outlet:

$$\left\{\frac{\partial C}{\partial z}\right\}_{(1,\theta)} = 0 \tag{31}$$

The set of equations describing the separation process in the chromatography column for the different models were solved numerically in the same way as described above for the set of the stirred tank equations.

4. Results and discussion

4.1. Adsorption equilibrium data

The Langmuir isotherm (Eq. (32)) was used to fit the experimental adsorption isotherm data of hIgG on both PG 700 and PG 1000 (Fig. 1). The Langmuir model relates the antibody concentration in the media (Q^*) at equilibrium with the antibody concentration in the bulk liquid phase (C^*). The isotherm is defined as:

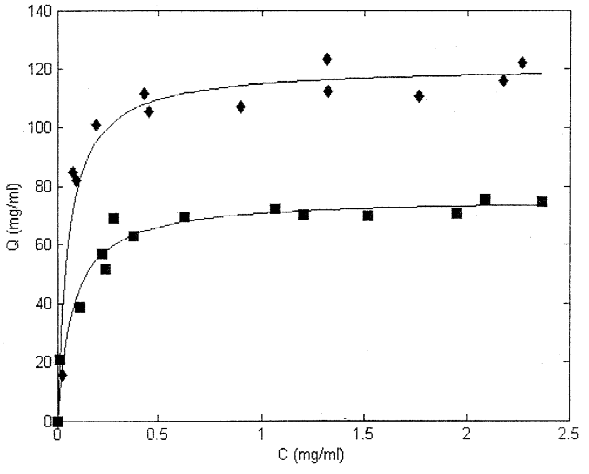

Fig. 1. Adsorption equilibrium data (hIgG adsorbed per unit particle volume) on PG 700 (♦) and PG 1000 (■) from PBS. Lines represent the Langmuir isotherm model (Eq. (32)) with the parameters presented in Table 2.

Table 2
Langmuir model parameters and dynamic capacity parameters for hIgG in PBS (pH 7.4). The parameters were identified from the correlation of the experimental data using Eqs. (32) and (33)

	PG 700	PG 1000
Langmuir model parameters		
Q_m (mg/ml bed)	69	42
Q_m (mg/ml media)	121	76
Q_m (mg/ml solid)	383	246
K_L (ml/mg)	18.9	13.1
Dynamic capacity parameters (10% breakthrough)		
Q_d^{∞} (mg/ml bed)	65	33
τ_d (min)	1.3	0.7

$$Q^* = \frac{Q_m K_L C^*}{1 + K_L C^*} \tag{32}$$

where Q_m is the maximum adsorption capacity and K_L is the Langmuir equilibrium constant (Table 2). PG 700 and PG 1000 strongly adsorb hIgG, approaching the monolayer capacity at hIgG concentrations $\geq$0.5 mg/cm^3. The higher static capacity achieved by PG 700 can be attributed to the fact that this media is prepared using a support with a higher specific surface area (~ 35 m^2/g, see Table 1). Assuming that a similar ligand density (g protein-A/m^2) is attained for both PG 700 and PG 1000, it follows that a larger capacity should be expected for the media having a larger specific surface area.

4.2. Stirred tank protein uptake kinetics

Stirred tank hIgG adsorption kinetics were measured on PG 700 (Fig. 2a) and PG 1000 (Fig. 2b) using initial hIgG concentrations of 0.1–3.0 mg/cm^3. The smaller pore size of PG 700 resulted in longer equilibration times. Using an initial hIgG concentration of 1.0 mg/cm^3, PG 1000 achieved equilibration after ~80 min, compared to PG 700 which required >140 min. Both media displayed similar behaviour for increasing initial hIgG concentrations. Adsorption rate increased with initial hIgG concentrations up to ~1.0 mg/cm^3. However, at hIgG concentrations $\geq$2.0 mg/cm^3, the uptake rate became less dependent on the initial hIgG concentration, as indicated by the proximity of the

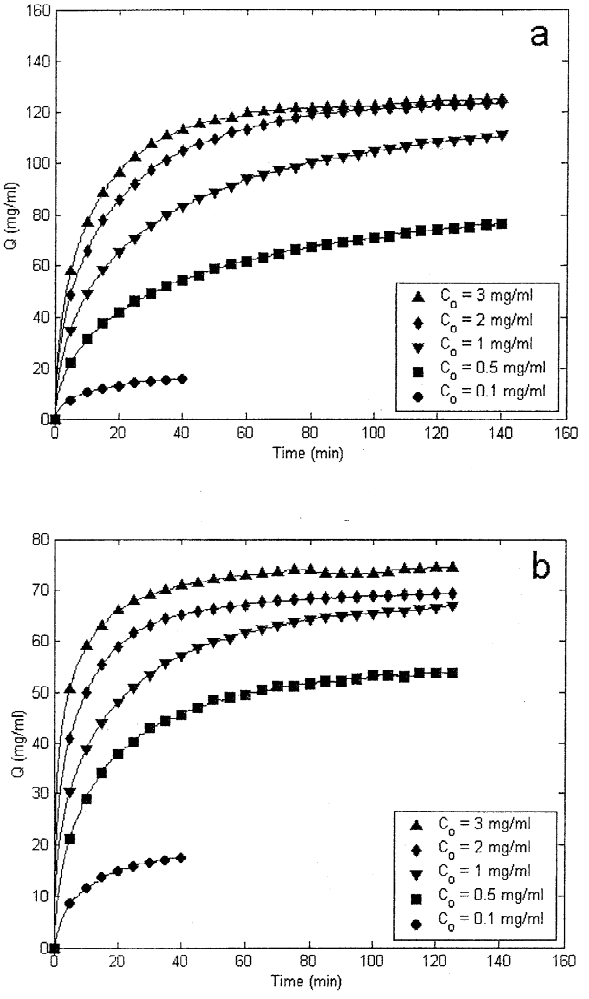

Fig. 2. Experimental stirred tank kinetics (hIgG adsorbed per unit particle volume) on (a) PG 700 and (b) PG 1000 in PBS using different initial hIgG concentrations. Both symbols and lines represent experimental data.

adsorption profiles. Such behaviour in adsorption kinetics has been reported by previous authors [14], and was explained in terms of the homogeneous model for protein diffusion within the media.

The experimental concentration profiles were approximated by the different models described above. The identified parameters are reported in Tables 3–5.

As expected, larger values of the effective diffusion coefficient are obtained for the 1000 Å material, by either using the pore diffusion or the homogeneous diffusion models. The same trend is observed

Table 3
Effective diffusion coefficients and residual sum of squares (RSS) identified from the fitting of the experimental uptake data using the pore diffusion model. The RSS was calculated as the sum of the squares of the differences between the experimental concentration in the bulk liquid phase and the calculated (by the model) concentration in the bulk liquid phase

Initial tank concentration (mg/ml)	PG 700		PG 1000	
	$D_p \cdot 10^7$ (cm^2/s)	RSS (mg^2/ml^2)	$D_p \cdot 10^7$ (cm^2/s)	RSS (mg^2/ml^2)
0.1	5.1		81	
0.5	1.8		2.0	
1.0	1.6	3.14	2.3	23.26
2.0	1.2		1.0	
3.0	1.0		1.2	
0.1–3.0	1.4	9.84	1.7	37.66

by either (i) fitting experimental data obtained from one particular initial concentration or (ii) simultaneously fitting the experimental data at all initial concentrations to a single diffusion coefficient. This result is consistent with the observation of longer equilibration times for PG 700 in the stirred tank experiments (Fig. 2).

A better fit of the experimental data was obtained for both media using the pore diffusion model than with the homogeneous diffusion model, as indicated by the smaller residual sum-of-squares (RSS) values (Tables 3 and 4). The pore diffusion model identifies a diffusion coefficient ~100 times faster than the one obtained from the homogeneous diffusion model on both media. When the same set of experimental uptake data was fitted using these two models, Martin et al. [23] found the effective diffusivity derived from the pore diffusion model to be ~100

Table 4
Effective diffusion coefficients and residual sum of squares (RSS) identified from the fitting of the experimental uptake data using the homogeneous diffusion model

Initial tank concentration (mg/ml)	PG 700		PG 1000	
	$D_{eff} \cdot 10^9$ (cm^2/s)	RSS (mg^2/ml^2)	$D_{eff} \cdot 10^9$ (cm^2/s)	RSS (mg^2/ml^2)
0.1	0.3		8.0	
0.5	0.4		1.0	
1.0	1.0	7.85	2.0	13.12
2.0	1.9		2.4	
3.0	2.8		5.0	
0.1–3.0	1.6	72.80	2.8	35.54

Table 5
Model parameters and residual sum of squares (RSS) identified from the fitting of the experimental uptake data using the surface layer model with the two different models to describe mass transport within the core

Core model	PG 700			PG 1000		
	δ/Rp	$D_{eff}\cdot 10^7$ or $D_p\cdot 10^7$ (cm^2/s)	RSS (mg^2/ml^2)	δ/Rp	$D_{eff}\cdot 10^7$ or $D_p\cdot 10^7$ (cm^2/s)	RSS (mg^2/ml^2)
Homogeneous diffusion	0	0.016	72.80	0.09	0.017	28.65
Porous diffusion	0.02	1.3	9.52	0.07	1.2	33.45

Note: $Rp = 50$ microns.

times larger than that obtained using the homogeneous diffusion model. The free solution diffusivity of hIgG is $\sim 4\cdot 10^{-7}$ cm^2/s [24], indicating that the diffusion of hIgG within the porous media is not significantly hindered, judging by the values of the effective diffusivities estimated using the pore diffusion model (Tables 3 and 4).

In terms of the pore diffusion model, the values of the effective diffusion coefficient ($1.0–2.0\cdot 10^{-7}$ cm^2/s) obtained for the porous glass materials are larger than the coefficients obtained using the same model for agarose-based materials ($0.1–1.0\cdot 10^{-7}$ cm^2/s), as reported elsewhere [11].

Overall, some improvement of the fitting was obtained when using the surface layer model that uses the pore diffusion to describe the mass transport at the particle's core (see Tables 3–5).

When fitting the surface layer model, similar values of the effective diffusivity are obtained at the core for either 700 Å or 1000 Å materials, irrespective of the nature of the model used to describe mass transport at the core—porous diffusion or homogeneous diffusion. A thicker surface layer was identified for the 1000 Å material. Thus, within the scope of the surface layer model, a larger fraction at the surface of the 1000 Å particle is solely limited by the rate of external film mass transfer. Within the framework of this model, a thicker surface layer accounts for the faster experimental rate of uptake observed for the 1000 Å material.

Theoretical profiles were calculated using the surface layer model that assumes pore diffusion holds at the particle's core. The calculated and experimental profiles are presented for PG 700 (Fig. 3a) and PG 1000 (Fig. 3b). Note that this model provides a good representation of the experimental data for each media tested using different initial hIgG concentrations.

4.3. Packed bed breakthrough profiles

Further insight into the separation process was obtained by examining the hIgG breakthrough profiles. Experimental breakthrough profiles were compared to the calculated curves using the models described above. The values of the surface layer thickness and the effective diffusivity obtained from the analysis of the stirred tank experiments were used to describe intraparticle mass transport in the packed bed.

Experimental band profiles were measured for several column heights (5–20 cm) and feed velocities (250 and 500 cm/h) for both PG 700 (Fig. 4) and PG 1000 (Fig. 5). Theoretical band profiles were calculated for the given experimental conditions using the different models and are also presented in Figs. 4 and 5. Overall, the models based on the pore diffusion mechanism provide a better representation of the experimental band profiles than the models based on the homogeneous diffusion mechanism.

The surface layer model that uses pore diffusion to describe mass transport at the core of the particle was then used to calculate breakthrough curves at different residence times. Prediction of the dynamic capacity using this particular model could be useful in process design, since it provides an estimation of the performance under various operating conditions. Dynamic capacities at 10% breakthrough were esti-

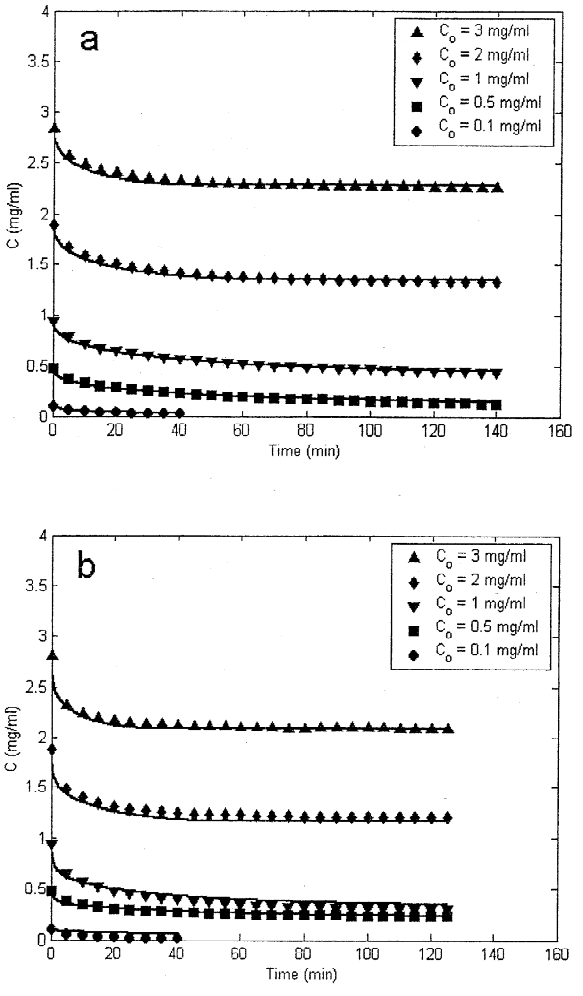

Fig. 3. Experimental stirred tank kinetics (hIgG bulk fluid concentration) on (a) PG 700 and (b) PG 1000 in PBS for different initial concentrations (symbols). Curves (lines) were calculated using the surface layer model that uses pore diffusion to describe mass transport at the particle's core.

mated from the calculated profiles. Reasonable agreement was found between experimental and calculated values for residence times of 0–10 min as shown for PG 700 (Fig. 6) and PG 1000 (Fig. 7).

4.4. Dynamic capacity

Experimental dynamic capacities ($Q_{d,10\%}$) of PG 700 (Fig. 8) and PG 1000 (Fig. 9) were evaluated at 10% antibody breakthrough (1.0 mg/cm^3 in feed) as a function of residence time (T_R) using several column heights (5–35 cm), diameters (0.6, 1.1 cm), and feedstock sources (SeraCare, Sigma). The following empirical model was used to fit these experimental data:

$$Q_d = \frac{Q_d^\infty \tau}{\tau_d + \tau} \tag{33}$$

where τ_d is a residence time constant and Q_d^∞ is the 10% breakthrough dynamic capacity at long residence times. From the correlation, Q_d^∞ values of 65 mg/cm^3 (PG 700) and 33 mg/cm^3 (PG 1000) were estimated (Table 2). Other correlations between dynamic capacity and residence time have been published elsewhere [7–9]. These expressions provide a very convenient way of data representation, especially in relation to the calculation of production rate (see below). Note in Figs. 8 and 9 that the experimental values of the dynamic capacity fall within the same curve even for different column geometries and antibody sources. The two media have similar dynamic capacities at residence times <1.0 min, before diverging at longer residence times. As expected, the dynamic capacity of PG 700 is larger than for PG 1000 at residence times >1.0 min, possibly a result of the fact that the media with the smaller pore size has a larger static capacity (Fig. 1). Moreover, at longer residence times the protein can diffuse further within the media and reach a greater number of adsorption sites within the particle with the smaller pore size.

4.5. Packed bed permeability

The pressure drop in a packed bed (ΔP) can be represented by the Blake–Kozeny expression [25]:

$$\Delta P = \frac{u_s \mu L}{k_o d_p^2} \tag{34}$$

where k_o is the specific column permeability. Eq. (34) can be rearranged as:

$$\frac{\Delta P}{L} = \gamma u_s \tag{35}$$

where

$$\gamma = \frac{\eta}{k_o d_p^2} \tag{36}$$

is an apparent friction constant.

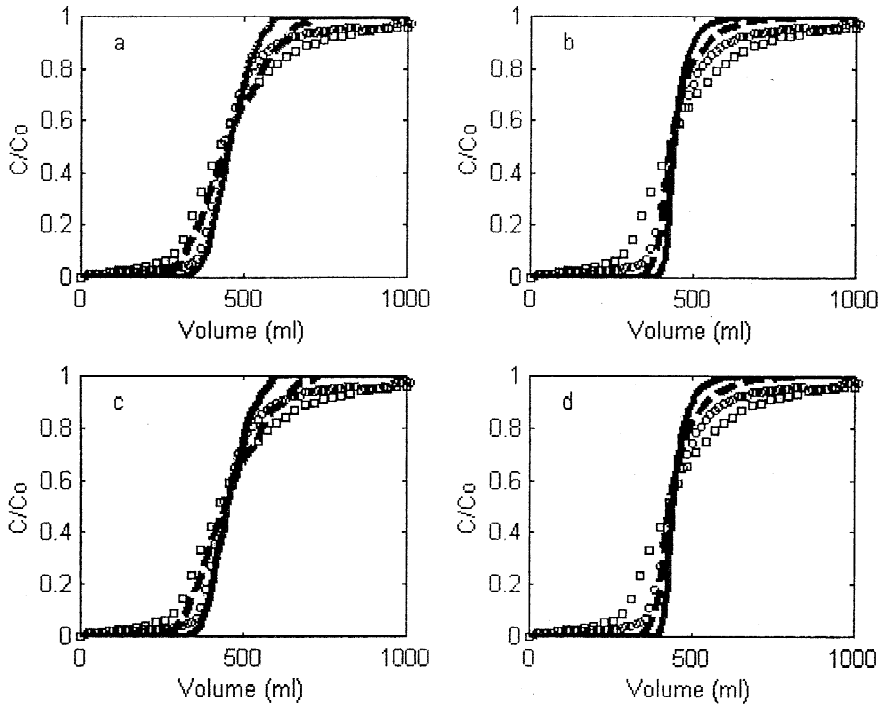

Fig. 4. Experimental (○ is 250 cm/h and □ is 500 cm/h) and calculated (solid line is 250 cm/h and dashed line is 500 cm/h) breakthrough profiles of hIgG on PG 700. The models used were the pore diffusion model (a), the homogeneous diffusion model (b), the surface layer model using pore diffusion to describe mass transport within the core (c), and the surface layer model using homogeneous diffusion to describe mass transport within the core (d). The feed was 1.0 mg/cm^3 of hIgG in PBS (pH 7.4). The column height was 20 cm.

Pressure drop per unit bed length (bar/cm) was measured as a function of linear velocity (200–1500 cm/h) for PG 1000 using process-scale columns (9–44 cm I.D.) and different bed heights (15–75 cm), as shown in Fig. 10. The experimental data was well approximated by Eq. (21) with a value of $\gamma = 4 \cdot 10^{-5}$ bar h/cm^2. The high permeability of PG 1000 can be attributed to the relatively large particle size (~100 μm) and the incompressible nature of the media backbone. PG 700 is assumed to have the same permeability since it has the same particle size.

4.6. Production rate

Production rates (P_r) for different hIgG feed concentrations and load residence times were calculated for both PG 700 and PG 1000 (Fig. 11) using the expression [7,8]:

$$P_r = \frac{1}{1000 \cdot \left(\frac{1}{C_o U_L} + \frac{N}{Q_d U_E} \right)} \tag{37}$$

Production rate depends upon five factors: dynamic capacity (Q_d); protein concentration in the feed (C_o); number of column volumes for bed regeneration, including wash, elute, clean and equilibration steps (N); load velocity (U_L); and regeneration velocity (U_E). Twenty ($N = 20$) column volumes were assumed for regeneration. The correlations obtained using Eq. (33) were used to estimate the dynamic capacity as a function of residence time for both media. A maximum pressure drop of 1.5 bar across the bed was set as a constraint in order to calculate (from Eq. (35)) the maximum velocity (1875 cm/h) allowed for the particular bed height under consideration (20 cm). The combination of the maximum velocity and the bed height produces a

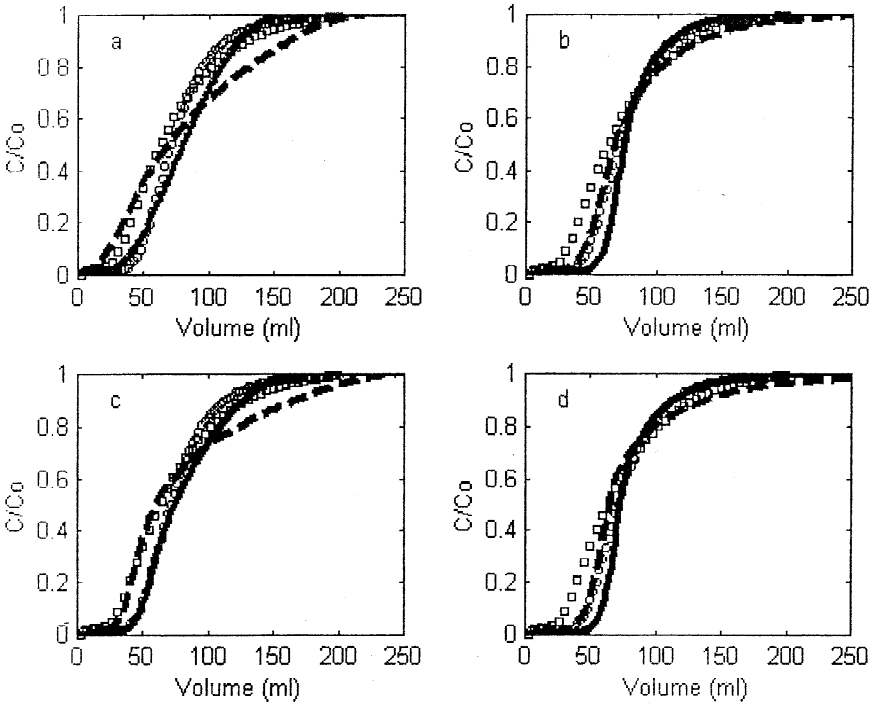

Fig. 5. Experimental (○ is 250 cm/h and □ is 500 cm/h) and calculated (solid line is 250 cm/h and dashed line is 500 cm/h) breakthrough profiles of hlgG on PG 1000. The models used were the pore diffusion model (a), the homogeneous diffusion model (b), the surface layer model using pore diffusion to describe mass transport within the core (c), and the surface layer model using homogeneous diffusion to describe mass transport within the core (d). The feed was 1.0 mg/cm^3 of hIgG in PBS (pH 7.4). The column height was 6.0 cm.

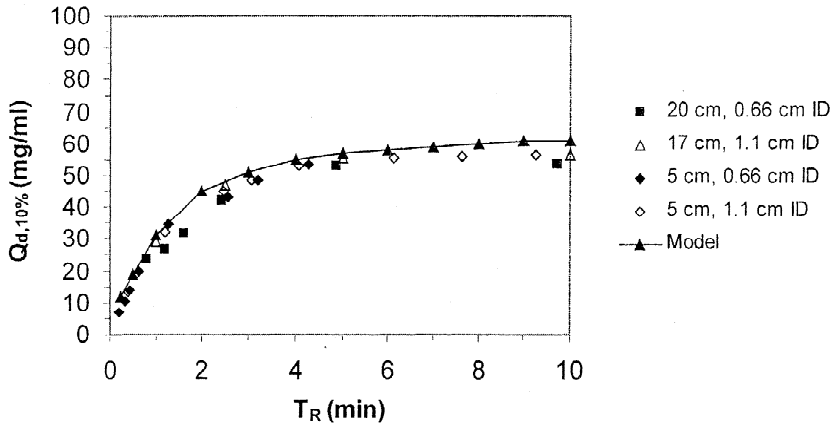

Fig. 6. Comparison of experimental and predicted column dynamic capacity at 10% breakthrough for PG 700 as a function of the residence time. The surface layer model that uses pore diffusion to describe mass transport at the particle's core was used to perform the model calculations. The feed was 1.0 mg/cm^3 hIgG in PBS (pH 7.4). The column heights were 5–20 cm. The column I.D.s were 0.66 and 1.1 cm.

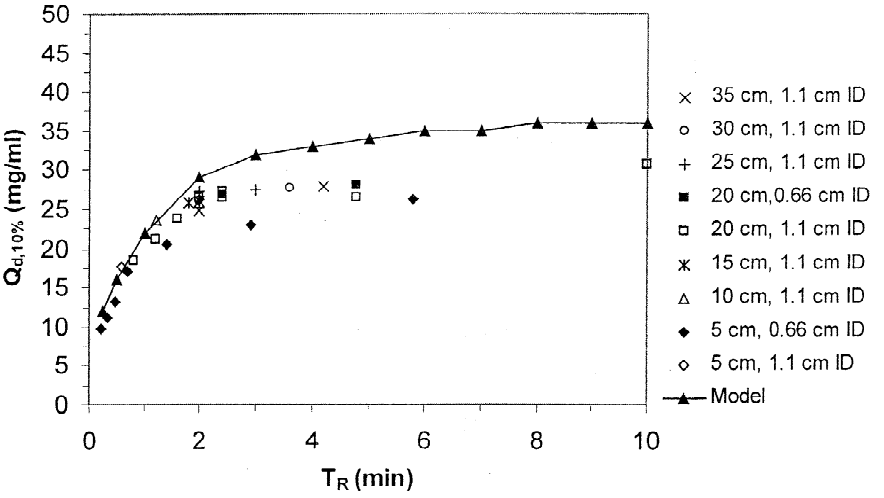

Fig. 7. Comparison of experimental and predicted column dynamic capacity at 10% breakthrough for PG 1000 as a function of the residence time. The surface layer model that uses pore diffusion to describe mass transport at the particle's core was used to perform the model calculations. The feed was 1.0 mg/cm^3 hIgG in PBS (pH 7.4). The column heights were 5–35 cm. The column I.D.s were 0.66 and 1.1 cm.

boundary at the minimum residence time (0.64 min). Accordingly, no throughput values are reported below 0.64 min.

Production rate contour plots show that PG 700 and PG 1000 (see Fig. 11) achieved similar production rates at hIgG feed concentrations $\leq$1.0 mg/cm^3. At a residence time of 2.4 min (which corresponds to a 20-cm bed operated at a linear velocity of 500 cm/h), PG 700 achieved only a slightly higher production rate (0.44 g/h/cm^2), than PG 1000 (0.41 g/h/cm^2). However, as the hIgG feed concentration increases, the production rate for PG 700 became greater than for PG 1000. At a hIgG feed concentration of 2.0 mg/cm^3 and residence time of 2.4 min, PG 700 had a production rate 14% greater (0.80 g/h/cm^2) than PG 1000 (0.70 g/h/

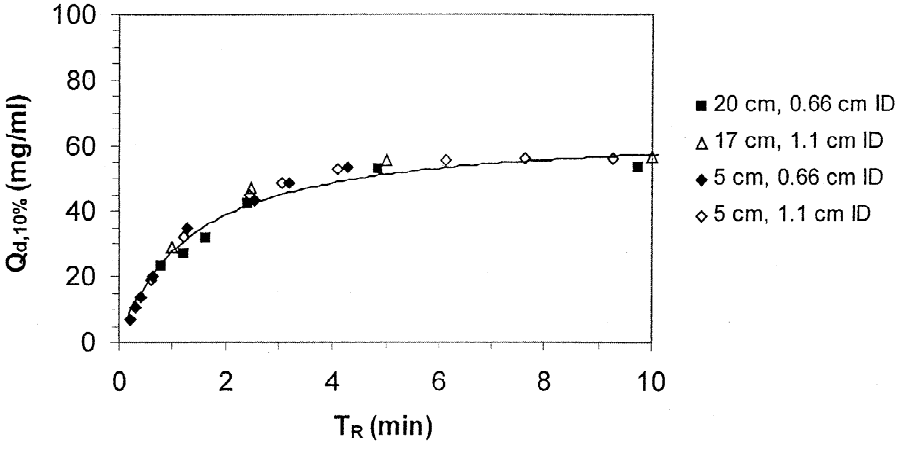

Fig. 8. Dynamic capacity at 10% breakthrough as a function of residence time on PG 700. Both SeraCare and Sigma materials were used as antibody sources for feedstock preparation. The line represents the fit of the experimental data to Eq. (33) with the parameters presented in Table 2. Feed: 1.0 mg/cm^3 hIgG in PBS.

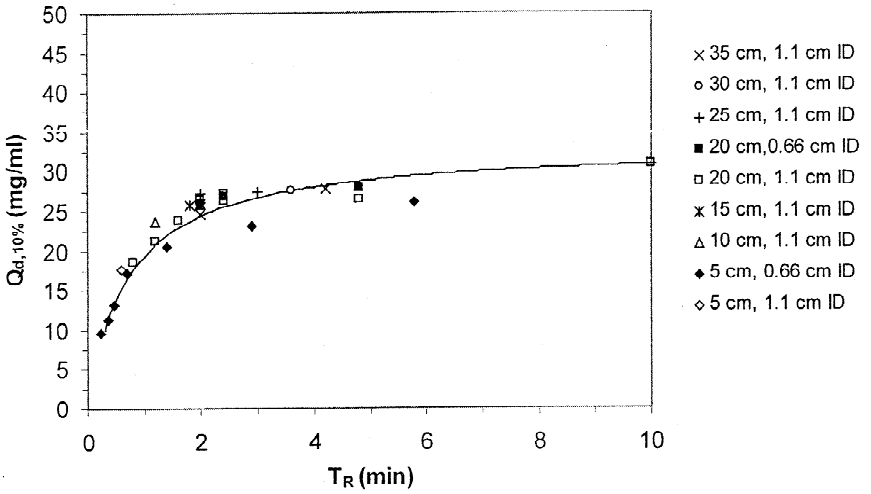

Fig. 9. Dynamic capacity at 10% breakthrough as a function of residence time on PG 1000. Both SeraCare and Sigma materials were used as antibody sources for feedstock preparation. The line represents the fit of the experimental data to Eq. (33) with the parameters presented in Table 2. Feed: 1.0 mg/cm^3 hIgG in PBS.

cm^2). Accordingly, for feedstocks containing antibody concentrations >1.0 mg/cm^3 the use of PG 700 could be advantageous in terms of a higher production rate relative to PG 1000.

5. Conclusions

Using hIgG as a feed, we examined the effect of the media pore size (700 Å and 1000 Å) on the

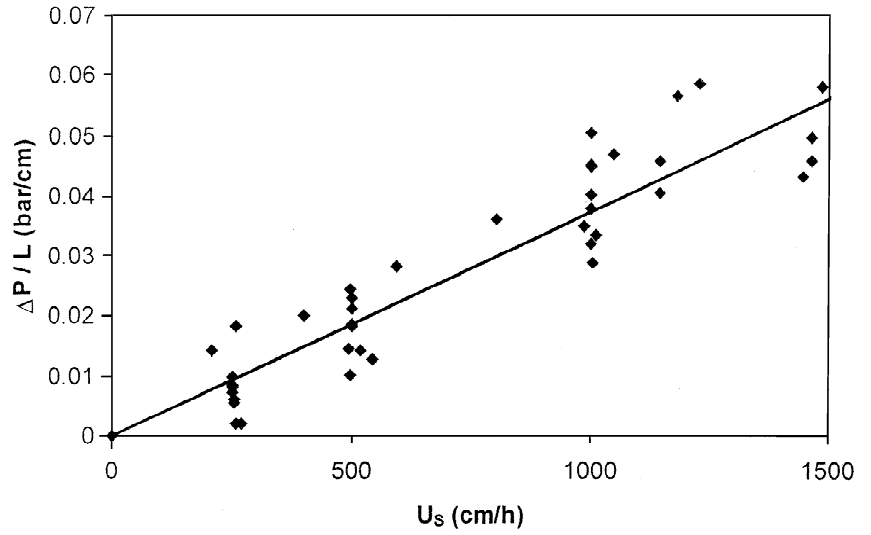

Fig. 10. Pressure drop vs. superficial velocity for PG 1000. The slope of the straight line fit ($R^2 = 0.8533$) represents the apparent friction constant ($4 \cdot 10^{-5}$ bar h/cm^2) of the media. Process-scale columns with bed heights in the range of 15–75 cm and diameters in the range of 9–44 cm were used in the experiments.

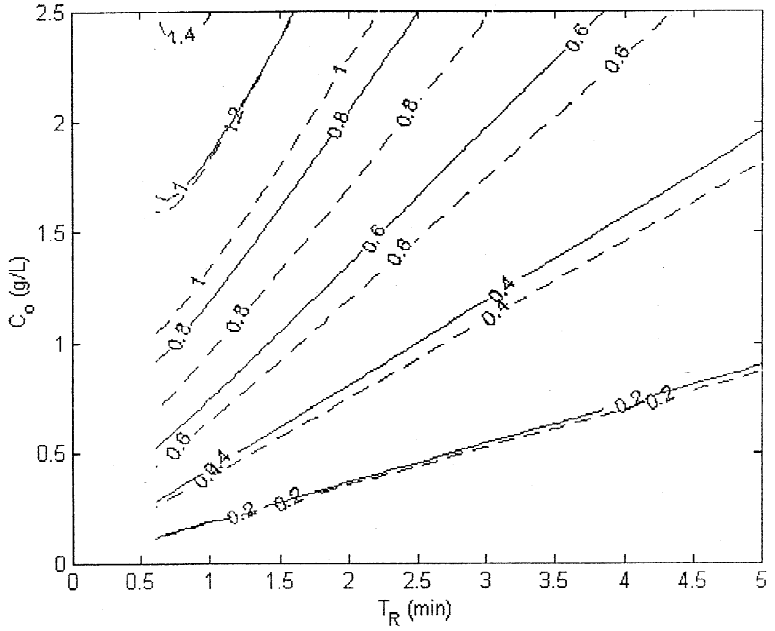

Fig. 11. Contour plots representing the production rate ($g/h/cm^2$) of PG 700 (dotted lines) and PG 1000 (solid lines) as a function of both residence time and hIgG feed concentration for a bed height of 20 cm.

purification performance. The use of a smaller pore size support resulted in an increase of both the equilibrium and dynamic capacity. The higher capacity of PG 700 might be related to the higher specific surface area and associated higher ligand concentration of this media. Adsorption equilibrium data for both media were properly correlated via the Langmuir isotherm model.

Protein uptake was found to be slower in PG 700 than in PG 1000 due to the smaller pore size. By using a surface layer model for intraparticle transport, a concentration-independent effective diffusivity was calculated for both media. When using the pore diffusion model to represent intraparticle mass transport, the effective hIgG diffusivity was found to be of the same order of magnitude as the free solution diffusivity ($\sim 10^{-7}$ cm^2/s), indicating that the diffusion inside the pores is not significantly hindered.

Using intraparticle transport parameters obtained from the stirred tank experiments, breakthrough profiles were calculated and dynamic capacities were estimated for different operating conditions. Reasonably good agreement was found between calculated and experimental breakthrough data. Such predictions could be helpful in order to evaluate the purification performance of the protein-A media in process-scale applications.

The selection of a particular chromatography media depends upon the specific purification requirements. Important factors to consider include protein size and concentration, dynamic capacity requirements, permeability, throughput, and cost of purification. For the specific antibody tested in this study, production rate of PG 700 was similar to PG 1000 for hIgG feed concentrations <1.0 mg/cm^3. Accordingly, the use of a protein-A media with a higher ligand concentration might not be necessary. However, as the trend toward higher antibody titres in cell culture continues, the use of media with a higher capacity (PG 700) could be advantageous in the future. The use of PG 700 might also be advantageous for the purification of species (containing a Fc IgG region) smaller than hIgG. A smaller protein should diffuse faster within the pore network of the media and, as a result, a larger value of the dynamic

capacity should be expected. Finally, additional studies using monoclonal antibodies will be required to expand the evaluation presented here and to test the generality of the presented conclusions.

Acknowledgements

We thank Purav Dave (Millipore Corp.) for assistance with the experimental measurements, as well as Katy Angus (Millipore Corp.) and Glen Bolton (Millipore Corp.) for useful discussions. We are also grateful to Ron Poling, Paul O'Neil, Steven Pearl and Ralf Kuriyel (all from Millipore Corp.) for their technical discussions.

References

[1] G. Subramanian (Ed.), Process Scale Liquid Chromatography, VCH, Weinheim, 1995.
[2] J.R. Birch, J. Bonnerjea, S. Flatman, S. Vranch, in: J.R. Birch, E.S. Lennox (Eds.), Monoclonal Antibodies: Principles and Applications, Wiley–Liss, New York, 1995, p. 231.
[3] K. Grant, B.G. Turner, in: J.N. Grindley, J.E. Ogden (Eds.), Understanding Biopharmaceuticals–Manufacturing and Regulatory Issues, Interpharm Press, Denver, 1999.
[4] J. Walter, in: M. Kastner (Ed.), Protein Liquid Chromatography (Journal of Chromatography Library Vol. 61), Elsevier, Amsterdam, 2000.
[5] A. Schwarz, in: P. Bailon, G.K. Ehrlich, W.-J. Fung, W. Berthold (Eds.), Affinity Chromatography: Methods and Protocols, Humana Press, Totowa, NJ, 2000.
[6] G.S. Blank, G. Zapata, R. Fahrner, M. Milton, C. Yedinak, H. Knudsen, C. Schmelzer, Bioseparation 10 (2001) 65.
[7] R.L. Fahrner, D.H. Whitney, M. Vanderlaan, G.S. Blank, Biotech. Appl. Biochem. 30 (1999) 121.
[8] R.L. Fahrner, H.V. Iyer, G.S. Blank, Bioprocess Eng. 21 (1999) 287.
[9] R.L. Fahrner, G.S. Blank, G.A. Zapata, J. Biotechnol. 75 (1999) 273.
[10] K. Biedermann, M. Sabater, J. Sørensen, H. Fiedler, C. Emborg, Bioseparation 2 (1991) 309.
[11] B.J. Horstmann, H.A. Chase, Chem. Eng. Res. Des. 67 (1989) 243.
[12] CPG Inc., 2002/2003 Product Catalog.
[13] A.K. Hunter, G. Carta, J. Chromatogr. A 897 (2000) 81.
[14] L.E. Weaver, G. Carta, Biotechnol. Prog. 12 (1996) 342.
[15] I. Quiñones-Garcia, I. Rayner, P.R. Levison, N. Dickson, G. Purdom, J. Chromatogr. A 908 (2001) 69.
[16] H.-S. Tsou, E.E. Graham, AIChE J. 31 (1985) 1959.
[17] B.H. Arve, A.I. Liapis, Biotechnol. Bioeng. 32 (1988) 616.
[18] A. Tongta, A.I. Liapis, D.J. Siher, J. Chromatogr. A 686 (1994) 21.
[19] G.L. Skidmore, B.J. Horstmann, H.A. Chase, J. Chromatogr. 498 (1990) 113.
[20] C.J. Geankoplis, Transport Processes and Unit Operations, 2nd. ed., Allyn and Bacon, Boston, MA, 1983.
[21] S.C. Foo, R.G. Rice, AIChE J. 21 (1975) 1149.
[22] A.M. Athalye, S.J. Gibbs, E.N. Lightfoot, J. Chromatogr. 589 (1992) 71.
[23] C. Martin, A. Ubiera, G. Iberer, G. Carta, Protein Adsorption on Agarose and Dextran-Grafted Ion-Exchange Media, presented at PREP' 2002, Washington, DC, 2002.
[24] M.T. Tyn, T.W. Gusek, Biotechnol. Bioeng. 35 (1990) 327.
[25] R.B. Bird, W.E. Stewart, E.N. Lightfoot, Transport Phenomena, Wiley, New York, 1963.